Limnol. Oceanogr., 55(6), 2010, 2585–2596

doi:10.4319/lo.2010.55.6.2585

The role of net community production in air–sea carbon fluxes at the North Pacific subarctic–subtropical boundary region

Evan Howard,* Steven Emerson, Seth Bushinsky, and Charles Stump

University of Washington School of Oceanography, Seattle, Washington

Abstract

The North Pacific subarctic–subtropical boundary region is an important sink for atmospheric CO_2, with high annual influx relative to surrounding waters and large seasonal variability. The location of the subarctic–subtropical gyre boundary is relatively stable, but there is a large seasonal migration of the North Pacific Chlorophyll Front, between ~ 30°N and ~ 45°N. To determine the role of biological productivity on the seasonal CO_2 flux, we measured sections of oxygen–argon gas ratios on cruises across the transition zone in November 1997 (autumn) and September 2008 (summer). A simple upper ocean model was used with the O_2 : Ar data to estimate the net community production (NCP) in the euphotic zone. On both cruises the NCP was highest at the chlorophyll front with average values from 30°N to 45°N of 3.4 ± 2.0 and 8.1 ± 2.7 mmol C m^{-2} d^{-1} in autumn and summer, respectively. These values are sufficient to make biologically induced carbon export an important component of the CO_2 drawdown in this region. Processes that control the relatively high NCP at this boundary are not certain, but it has been demonstrated that horizontal convergence of nitrate plays some role.

The oceanic response to anthropogenic carbon dioxide input to the atmosphere is an important scientific and social focus due to the potentially significant effects of increasing atmospheric partial pressure of CO_2 (pCO_2) on ecology and economies globally. The sum of biologically mediated processes affecting the fixation of CO_2 and export of carbon from the euphotic zone to the deep ocean is a major control on atmospheric pCO_2. This mechanism of carbon export from the surface ocean is known as the biological carbon pump (Volk and Hoffert 1985). Our focus in this paper is the North Pacific Ocean where the pCO_2 drawdown at the subarctic–subtropical boundary causes an annual influx of carbon to the ocean (1.8–2.9 mol C m^{-2} yr^{-1}) that is roughly equal to the carbon efflux to the atmosphere in the equatorial Pacific (Zeng et al. 2002; Takahashi et al. 2009). The carbon drawdown has a dramatic seasonal variation, and is strongest in autumn and weakest in summer (Zeng et al. 2002). In spite of the global importance of this CO_2 sink, there is uncertainty about the importance of biological and physical mechanisms that affect carbon exchange in this region of the ocean. The present balance between these forcings must be better understood to evaluate how changing climate might affect carbon fluxes in this region.

We report measurements from two cruises crossing the subarctic–subtropical boundary region with the express purpose of determining the importance of biological processes in creating an ocean sink for atmospheric CO_2. The cruises were conducted ~ 10 yr apart aboard the R/V *Thomas G. Thompson*, in November of 1997 (TTN072) and September 2008 (TTN224). We refer to these two cruises throughout the paper as UWStu97 and UWStu08, respectively. This paper uses background hydrography, determinations of upper-ocean oxygen and argon concentrations, and a simple mass balance model to yield estimates of biologically produced oxygen from which we infer the seasonal pattern of net community production (NCP) across the subtropical–subarctic boundary. NCP is the difference between net photosynthesis and respiration in the biological community of a water parcel. At steady state (no increase in organic matter in the water parcel), NCP should equal the flux of organic carbon from the euphotic zone to the deep ocean, or carbon export (Emerson and Hedges 2008).

Methods

Background and previous work—A major feature in the surface ocean hydrography of the North Pacific Ocean is the salinity and temperature boundary referred to as the North Pacific Transition Zone, which follows the Kuroshio Extension Current, along ~ 43°N, until it diverges at ~ 155°W and curves south (Roden 1991; Aydin et al. 2004; Ayers and Lozier 2010). This physical boundary is characterized by two frontal zones containing one or more thermohaline fronts on either side of an intermediate region separating fresh, cool subpolar waters to the north and salty, warm subtropical waters to the south (Fig. 1; Lynn 1986; Roden 1991; Aydin et al. 2004). The northern frontal zone is bounded by the subarctic front along a climatological mean latitude of 43°N, and is identified by the outcropping of an isohaline of salinity 33.0, which forms the upper boundary of the permanent subarctic halocline between 120 m and 180 m (Roden 1991). The bottom of this halocline, the 33.8 isohaline, outcrops near 40°N and defines the southernmost extent of the northern frontal zone. The southern frontal zone lies between the outcroppings of the upper and lower limits of the subtropical halocline, at salinities of 34.8 near 34°N and 35.2 near 31°N, the subtropical front. Ekman currents converge at the two frontal zones, which generally do not vary from their mean climatological values by > 150–200 km (Roden 1991).

* Corresponding author: ehoward2@u.washington.edu

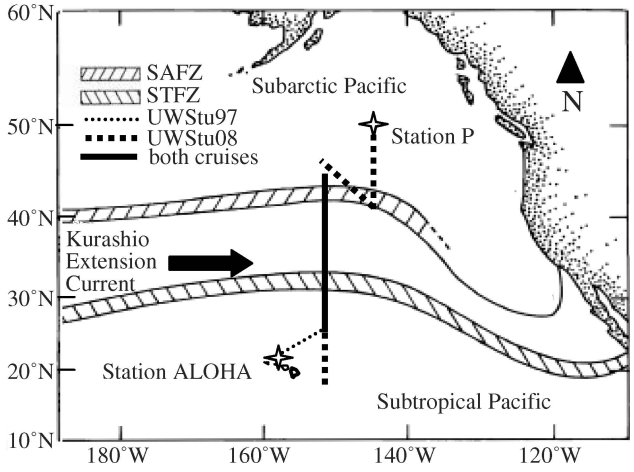

Fig. 1. The eastern North Pacific subarctic–subtropical boundary region, and mean climatological positions of the subarctic and subtropical frontal zones (SAFZ and STFZ), modified from Roden (1991). Sta. P, Sta. ALOHA, and UWStu97 and UWStu08 cruise tracks are indicated.

Large gradients in surface nutrients such as nitrate and phosphate span the transition zone between nutrient-rich (but iron-poor) conditions in the Alaskan Gyre to the north and nutrient-poor conditions in the North Pacific Subtropical Gyre to the south. Distinct planktonic communities are associated with the different nutrient and physical regimes in the subarctic, transition zone, and the subtropical ocean (Brinton 1962; Pearcy 1991). Large predators including squid (*Onychoteuthis* and *Ommastrephes*), albacore (*Thunnus*), and turtles (*Caretta*), track a transitory chlorophyll front through the transition zone in large numbers during north–south and east–west migrations, suggesting a large coincident food source (Laurs and Lynn 1991; Pearcy 1991; Polovina et al. 2001). However, the chlorophyll front and any associated productivity is not fixed relative to the physical transition zone, and instead shifts seasonally; chlorophyll *a* (Chl *a*) concentrations determined by satellite colorimetry remain greater than 0.2 mg m^{-3} north of 30°N in the boreal winter and decrease rapidly southward, while this boundary is nearer 40°N in the summer. We refer to this feature as the North Pacific Chlorophyll Front after Polovina et al. (2001) to distinguish it from the more stationary physical transition zone.

Photosynthesis along the chlorophyll front and cooling along the Kuroshio Extension Current and across the transition zone can both lead to low surface pCO_2. The combined effects of these biological and physical processes create the previously mentioned band of high CO_2 influx into the surface ocean (Takahashi et al. 2009). Relatively few data sets exist to differentiate physical and biological processes causing pCO_2 drawdown in the subarctic–subtropical boundary region, which includes both the North Pacific Transition Zone and the chlorophyll front (~ 30–45°N). A seasonal estimate of NCP in the region determined from nitrate drawdown is 14.6 mmol C m^{-2} d^{-1} (Mar–Sep; Wong et al. 2002), while a more recent volunteer observation ship (VOS)–based study using surface-water O_2 : Ar ratios estimated a value of 14.2 mmol C m^{-2} d^{-1} in the transition zone (Mar, Apr, Oct mean; Juranek 2007). Prior studies of the subtropical and subarctic North Pacific provide basin-scale context for these high NCP values. Published estimates from Sta. ALOHA (Fig. 1) using a variety of methods give an annual average subtropical NCP of 6.7 ± 2.6 mmol C m^{-2} d^{-1} (as summarized by Emerson et al. 2008). The annual average NCP in the eastern subarctic Pacific at Sta. P (Fig. 1) is estimated to be 5.8 ± 1.1 mmol C m^{-2} d^{-1} (as summarized by Emerson and Stump 2010). We use the data in this study to clarify the mechanisms of carbon flux and contrast the seasonal differences associated with the physical and biological frontal regions.

Field methods—Both cruise tracks followed 152°W south from ~ 46°N to ~ 20°N, with the more recent cruise going through a multileg transect that crossed the northern part of the North Pacific Transition Zone three times (Fig. 1). There were 10 and 14 stations sampled for gas tracers of biological production on UWStu97 and UWStu08, respectively (Table 1). Four or more depths were sampled at each station, ranging from the surface to ≥ 150 m. Frequent replicates were sampled to define analytical precision and accuracy.

In preparation for gas sampling, 250 mL glass flasks with Louwers–Hapert 9-mm valves were poisoned, evacuated, and the necks filled with CO_2 and capped to minimize atmospheric contamination, as described in Emerson et al. (1995). Water samples were taken at each cast by Niskin bottles on a Conductivity–Temperature–Depth (CTD) rosette. On sampling, ~ 130 mL of seawater was drawn into the evacuated flask from a Niskin bottle, with care taken to exclude air. The neck was then dried and filled with CO_2 for storage (Emerson et al. 1995).

Replicates of water from each sampled Niskin were titrated by the modified Winkler method to determine the oxygen concentration (Carpenter 1965). Discrete temperature, salinity, nutrients, and Chl *a* were sampled from the same Niskins, and analysis run on shipboard instruments using Joint Global Ocean Flux Study protocols (Knap et al. 1996). Temperature and salinity bottle measurements were used to calibrate the CTD data.

Analytical methods—Gas samples from these cruises were returned to the laboratory at the University of Washington, where each sample was weighed and submersed in a water bath at constant temperature for a minimum of 8 h to equilibrate gases between the water and head space. After most of the water was pumped out of the flask, the sample gas was cryogenically pumped through liquid nitrogen to remove CO_2 and remaining water vapor and frozen into a steel 'finger' in liquid helium. Samples from the more recent cruise were spiked with ^{36}Ar to determine Ar concentrations by isotope dilution. Each finger was then removed, left at room temperature for 4 h and the sample analyzed on a Finnigan 253 mass spectrometer to determine gas ratios. Atmospheric standards were run with samples from each station to calibrate the ^{36}Ar spike (Emerson et al. 1999).

Mass spectrometry-determined O_2 : Ar ratios and oxygen data from the Winkler titrations were used to obtain the

Table 1. Station coordinates, sample date, mixed-layer depths, and variables used to calculate the gas exchange term in Eq. 12. k_{O2} is the weighted mass transfer coefficient over the 60 d prior to sampling, where uncertainties are assumed to be ± 30% (Reuer et al. 2007; Emerson et al. 2008). $[O_2]^{sat}$ is the average oxygen concentration at saturation and $\Delta O_2 - \Delta Ar$ is the oxygen–argon supersaturation difference in the surface mixed layer. Uncertainties for these variables are calculated standard deviations from replicates. Uncertainties for the subarctic Pacific, transition zone, and subtropical Pacific are reported as standard errors in the mean.

Cruise	Latitude and longitude (°)	Sample date	Mixed layer (m)	k_{O2} (m d^{-1})	$[O_2]^{sat}$ (mmol m^{-3})	$\Delta O_2 - \Delta Ar$ (%)
UWStu97	45N,152W	07 Nov 1997	78	8.6±2.6	275.8±0.1	0.0±0.2
	43.7N,151.2W	07 Nov 1997	60	7.3±2.2	273.1±0.1	−0.4±0.2
	42.2N,152W	08 Nov 1997	68	16.9±5.1	264.9±0.1	0.3±0.2
	40N,152W	09 Nov 1997	67	6.1±1.8	252.5±0.1	0.1±0.2
	38N,152W	10 Nov 1997	57	7.6±2.3	244.7±0.1	0.4±0.2
	36N,152W	10 Nov 1997	50	9.5±2.8	235.3±0.1	0.5±0.2
	33N,152W	11 Nov 1997	54	6.3±1.9	229.2±0.1	0.5±0.2
	29N,152W	12 Nov 1997	50	4.0±1.2	216.4±0.1	0.5±0.2
	25N,152W	14 Nov 1997	76	4.6±1.4	213.2±0.1	0.7±0.2
	22.4N,158.1W	16 Nov 1997	79	6.1±1.8	208.9±0.2	0.5±0.2
North Pacific Transition Zone	(30–45°N)	—	—	8.9±1.4	254±6.9	0.2±0.2
Subtropical Pacific	(<30°N)	—	—	4.9±1.6	212.8±2.2	0.6±0.2
UWStu08	50.1N,144.8W	30 Aug 2008	35	4.2±1.3	276±1	3.3±0.2
	47N,152W	02 Sep 2008	35	4.4±1.3	269±1	1.8±0.2
	46N,150.6W	04 Sep 2008	13	3.8±1.1	266.0±0.2	2.2±0.2
	45N,152W	04 Sep 2008	25	4.2±1.3	257.2±0.5	2.6±0.2
	45N,149.9W	05 Sep 2008	30	3.9±1.2	262.4±0.5	3.5±0.2
	44N,149.2W	05 Sep 2008	30	3.8±1.1	247.9±0.5	0.6±0.2
	43N,148.5W	06 Sep 2008	50	3.1±0.9	247.1±0.5	0.7±0.2
	42N,152W	07 Sep 2008	35	3.7±1.1	241.0±0.1	0.2±0.2
	42N,145W	08 Sep 2008	30	3.9±1.2	244.7±0.5	0.2±0.2
	39N,152W	09 Sep 2008	20	3.2±0.9	227.6±0.5	0.3±0.2
	37N,152W	11 Sep 2008	25	3.1±0.9	216.0±0.3	0.3±0.2
	30N,152W	12 Sep 2008	40	3.1±0.9	210.9±0.1	0.8±0.2
	22N,152W	15 Sep 2008	50	3.7±1.1	206.3±0.5	0.7±0.2
	18N,152W	16 Sep 2008	45	3.9±1.2	208.9±0.3	0.3±0.2
Subarctic Pacific	(>42°N)	—	—	3.9±0.2	260.8±4.1	2.1±0.4
North Pacific Transition Zone	(32–42°N)	—	—	3.5±0.2	232.3±6.6	0.3±0.2
Subtropical Pacific	(<32°N)	—	—	3.6±0.2	208.7±1.3	0.6±0.2

argon concentration of each sample. This method is independently precise and accurate to ± 0.2% in surface waters where oxygen concentrations are high, with the largest uncertainty in the accuracy determined by the purity of the KIO_3 standard used in the Winkler titrations (Emerson et al. 1999). In the isotope dilution method used on UWStu08 samples, a known amount of ^{36}Ar spike was added to a sample, and the $^{36}Ar : {}^{40}Ar$ ratio was measured to determine the argon concentration in the sample. The largest uncertainty in this method is believed to be in determining the total amount of ^{36}Ar spike added to the flask, which should be accurate to better than ± 0.2% as well.

Relative standard deviations for oxygen and argon concentrations were calculated for each cruise as a measure of uncertainty, based on the mean standard deviation of all duplicate sample sets. UWStu97 concentrations used in this study, derived only from the Winkler-based method, had a standard deviation of ± 0.15%. UWStu08 gas concentration standard deviations from the Winkler and isotope dilution methods were both ± 0.1%. Values from UWStu08 derived from isotope dilution are interpreted here.

Gas concentrations from multiple depths within the surface mixed layer should be very similar. Five UWStu97 and five UWStu08 mixed-layer values that differed in both oxygen and argon concentration by more than two standard deviations from the mixed-layer mean were discarded, which amounted to 5% of the total samples on each cruise.

Mass balance model—Oxygen and argon gas measurements provide a means to determine the rate of NCP. We use a steady-state model of the mixed layer in isolation from deeper waters to determine the mixed-layer NCP in terms of oxygen, as well as a simple reservoir model of processes that happen below the mixed layer but within the euphotic zone. Our model assumes no vertical exchange between these two reservoirs or between the lower reservoir and the water below the top of the permanent pycnocline where the oxygen minimum begins. Thus, biological oxygen production in the deeper reservoir is, if anything, an underestimate. At the Hawaii Ocean Time–series, the error induced by assuming low vertical mixing may leave up to 40% of submixed-layer production unaccounted for (Hamme and Emerson 2006; Nicholson et al. 2008). Previous estimates of the depth distribution of oxygen production at Sta. ALOHA indicate production in the mixed layer accounts for 70–80% of the NCP (Emerson et al. 2008; Nicholson et al. 2008).

In the surface-ocean mixed layer of depth (h, m), the product of h and the time rate of change of concentration of gas C (d[C]/dt, mol m^{-3} d^{-1}) is equal to the sum of air–water gas exchange (F_{A-W}), horizontal advection (U), and the NCP by photosynthesis and respiration (J, mol m^{-2} d^{-1}), in the absence of vertical exchange. This can be written as the following mass balance:

$$h\frac{\partial[\mathrm{C}]}{\partial \mathrm{t}} = F_{\mathrm{A-W}} + U_{\mathrm{C}} + J_{\mathrm{C}} \quad (1)$$

The gas exchange flux is parameterized as the sum of interface diffusive exchange (G_C), and bubble processes:

$$F_{\mathrm{A-W}} = G_{\mathrm{C}} + B_{\mathrm{C}} \quad (2)$$

G_C is the product of a mass transfer coefficient, (k, m d^{-1}), and the difference between the measured concentration of gas, [C], and the concentration expected at saturation, $[C]^{sat}$ (mol m^{-3}).

$$G_{\mathrm{C}} = -k_{\mathrm{C}}\left([\mathrm{C}] - [\mathrm{C}]^{\mathrm{sat}}\right) \quad (3)$$

The bubble flux (B_C, mol m^{-2} d^{-1}) is caused by bubbles that enter the surface ocean during wave breaking and inject gas into the surface water. In a simple model where it is assumed that bubble overpressure does not significantly affect other constants, B_C has been parameterized into separate mechanisms for bubbles that totally dissolve when they enter the ocean, using a bubble injection transfer velocity (V_{inj}), and those that exchange gas in the water and reemerge to the atmosphere, using the exchange coefficient (V_{ex}):

$$B_{\mathrm{C}} = \left[V_{\mathrm{inj}} + V_{\mathrm{ex}}(D_{\mathrm{C}})^{1/2}\alpha_{\mathrm{C}}\right]p\mathrm{C} \quad (4)$$

where pC (Pa) is the partial pressure of the gas in the air, D (cm^2 s^{-1}) is the molecular diffusion coefficient of the gas, and α is the solubility coefficient (Fuchs et al. 1987; Hamme and Emerson 2006).

The mass transfer coefficient, k is normalized to the mass transfer coefficient for CO_2 at 20°C, k*, via the Schmidt number, S_c:

$$k_{\mathrm{C}} = k^* \mathrm{S}_{\mathrm{C}}^{-1/2} \quad \text{where} \quad \mathrm{S}_{\mathrm{C}} = \left(\frac{v}{D_{\mathrm{C}}}\right) \quad (5)$$

where v (cm^2 s^{-2}) is the kinematic viscosity of seawater. We calculate the Schmidt number using the coefficients of Wanninkhof (1992). The normalized mass transfer coefficient (k*) is empirically related to satellite wind-speed measurements via gas-exchange tracer experiments. In our application we calculate daily k values using satellite ocean wind-speed databases and the relationship derived by Nightingale et al. (2000). Daily k values from ≥ 30 d prior to sampling at each station are weighted and summed algebraically according to how close each is to the day of sampling and the fraction of the mixed layer ventilated, as described in Reuer et al. (2007). In practice, longer weighting periods (60 d) generally result in < 10% difference to the mass transfer coefficient (much less when winds are relatively stable), and are used only for UWStu97 because winds were more variable and satellite observation was more frequently blocked by clouds. Wind-speeds along the UWStu97 cruise path are obtained from the National Aeronautics and Space Administration's (NASA) Special Sensor Microwave Imager Version 6 database and UWStu08 values are obtained from NASA's Quick Scatterometer database.

The flux caused by advection (U), is determined from the spatial gradient of a gas (d[C]/dx), where x (m) is the horizontal distance scale, multiplied by the product of an advective flow rate (u, m d^{-1}) and the depth of the flow (Δz):

$$U_{\mathrm{C}} = u\Delta z\frac{\partial[\mathrm{C}]}{\partial x} \quad (6)$$

Although both wind-driven Ekman transport and geostrophic flow cause advection, we consider only the Ekman flow because it dominates in the mixed layer (Wijffels et al. 1994; Abell 2003). Flow rates are calculated from climatological wind data presented by da Silva et al. (1994).

Substituting Eqs. 2, 3, 4, and 6 into Eq. 1 and rewriting for argon and oxygen gives

$$h\frac{\partial[\mathrm{Ar}]}{\partial \mathrm{t}} = -k_{\mathrm{Ar}}\left([\mathrm{Ar}] - [\mathrm{Ar}]^{\mathrm{sat}}\right) + \left[V_{\mathrm{inj}} + V_{\mathrm{ex}}(D_{\mathrm{Ar}})^{1/2}\alpha_{\mathrm{Ar}}\right]\mathrm{pAr} + u\,\Delta z\frac{\partial[\mathrm{Ar}]}{\partial x} \quad (7)$$

$$h\frac{\partial[\mathrm{O_2}]}{\partial \mathrm{t}} = -k_{\mathrm{O2}}\left([\mathrm{O_2}] - [\mathrm{O_2}]^{\mathrm{sat}}\right) + \left[V_{\mathrm{inj}} + V_{\mathrm{ex}}(D_{\mathrm{O2}})^{1/2}\alpha_{\mathrm{O2}}\right]\mathrm{pO_2} + u\,\Delta z\frac{\partial[\mathrm{O_2}]}{\partial x} + J_{\mathrm{O2}} \quad (8)$$

where there is no production term for the inert gas argon. We assume steady state because each concentration profile was taken at a single point in time and there is no other option. Multiplying Eq. 7 by $[O_2]^{sat}/[Ar]^{sat}$ and subtracting it from Eq. 8 results in

$$\begin{aligned}\mathrm{J} = {} & k_{\mathrm{O2}}\left[[\mathrm{O_2}] - \left(1 - \frac{k_{\mathrm{Ar}}}{k_{\mathrm{O2}}}\right)[\mathrm{O_2}]^{\mathrm{sat}} - \left(\frac{k_{\mathrm{Ar}}}{k_{\mathrm{O2}}}\right)\left(\frac{[\mathrm{O_2}]^{\mathrm{sat}}}{[\mathrm{Ar}]^{\mathrm{sat}}}\right)[\mathrm{Ar}]\right] \\ & - V_{\mathrm{inj}}\,\mathrm{pO_2}\left(1 - \frac{\alpha_{\mathrm{O2}}}{\alpha_{\mathrm{Ar}}}\right) - V_{\mathrm{ex}}\,\mathrm{pO_2}\,\alpha_{\mathrm{O2}}\left[(D_{\mathrm{O2}})^{1/2} - (D_{\mathrm{Ar}})^{1/2}\right] \\ & - u\,z\left[\frac{\partial[\mathrm{O_2}]}{\partial x} - \frac{\partial[\mathrm{Ar}]}{\partial x}\left(\frac{[\mathrm{O_2}]^{\mathrm{sat}}}{[\mathrm{Ar}]^{\mathrm{sat}}}\right)\right] \end{aligned} \quad (9)$$

Oxygen and argon have very similar solubility and molecular diffusion coefficients. If they are assumed to be the same the above equation can be written as

$$\begin{aligned} J = {} & [\mathrm{O_2}]^{\mathrm{sat}}k_{\mathrm{O2}}\left(\frac{[\mathrm{O_2}] - [\mathrm{O_2}]^{\mathrm{sat}}}{[\mathrm{O_2}]^{\mathrm{sat}}} - \frac{[\mathrm{Ar}] - [\mathrm{Ar}]^{\mathrm{sat}}}{[\mathrm{Ar}]^{\mathrm{sat}}}\right) \\ & - u\,\Delta z[\mathrm{O_2}]^{\mathrm{sat}}\frac{\partial}{\partial x}\left(\frac{[\mathrm{O_2}] - [\mathrm{O_2}]^{\mathrm{sat}}}{[\mathrm{O_2}]^{\mathrm{sat}}} - \frac{[\mathrm{Ar}] - [\mathrm{Ar}]^{\mathrm{sat}}}{[\mathrm{Ar}]^{\mathrm{sat}}}\right) \end{aligned} \quad (10)$$

The degree of supersaturation of a gas (ΔC) is the difference between the measured and saturated concentrations ([C] and $[C]^{sat}$) divided by the gas concentration at saturation, and is usually presented as a percent:

$$\Delta C = \frac{[C] - [C]^{sat}}{[C]^{sat}} \times 100\% \quad (11)$$

A positive ΔC indicates supersaturation, while a sample with a negative percent is undersaturated. Argon is not influenced by biological activity but has similar physical characteristics as oxygen. Therefore, the difference in degree of saturation between the two gases corrects for changes in supersaturation caused by physical processes such as diffusion and bubbles created by breaking waves. Determining the excess oxygen saturation relative to argon yields an estimate of biologically produced oxygen over the 10–20-d residence time of oxygen in the mixed layer, where positive values indicate net oxygen production and net autotrophy (Craig and Hayward 1987; Spitzer and Jenkins 1989; Emerson et al. 1991). Substituting the above definition of saturation state into Eq. 10 results in the equation we use to determine NCP in the mixed layer in terms of biologically produced oxygen supersaturation:

$$J = [O_2]^{sat}\left[k_{O2}(\Delta O_2 - \Delta Ar) - u\,\Delta z\frac{\partial}{\partial x}(\Delta O_2 - \Delta Ar)\right] \quad (12)$$

This production estimate again represents an average for the 10–20 d prior to sampling, with the exact period most dependent on the mass transfer coefficient.

A first-order estimate of the NCP below the mixed layer defined by the seasonal pycnocline can be determined by assuming this region is a closed system (we assume mixing and advection are small with respect to in situ oxygen production) and that the build-up of O_2 has increased linearly with time since it was isolated from the mixed layer. With these assumptions, the NCP below the mixed layer (J_{sml}) can then be written as

$$J_{sml} = \int_{z_1}^{z_2} \frac{[O_2](\Delta O_2 - \Delta Ar)}{2\,t}\,dz \quad (13)$$

z_1 is the mixed-layer depth (m), below which oxygen accumulates. z_2 is the estimated greatest depth of the supersaturation maximum below which net respiration begins. The number of days that the gas has accumulated (t) is estimated based on the sample dates and the beginning of spring productivity as identified by a rapid rise in oxygen supersaturation, usually late April or early May near the transition zone (Emerson 1987). We use a geometric simplification of the above integral to solve for the amount of biologically produced oxygen below the mixed layer. This production estimate averages over the entire period of seasonal production, rather than the shorter residence time of oxygen in the mixed layer, and has larger uncertainties as light, mixed-layer depth, and biology vary on these time scales.

Results

Hydrography of the transition zone and chlorophyll front—Sections of temperature, salinity, oxygen concentration, and Chl *a* in the surface 150 m, and surface ocean nitrate and Chl *a* concentrations along 152°W are presented in Fig. 2. Temperature and salinity generally increase southwards, and the subarctic thermocline is stronger in the September cruise (Fig. 2a–d). Oxygen concentrations decrease from the subarctic to the subtropics, with the highest concentrations between the seasonal thermocline and the bottom of the subarctic halocline (Fig. 2e,f). Both oxygen and Chl *a* sections show subsurface fingers south of the subarctic, and the highest concentrations of both are roughly coincident (Fig. 2g–h). Surface nitrate concentrations generally decrease across the subarctic–subtropical boundary, with nitrate depletion ($\sim < 0.2$ μmol NO_3^- L^{-1}) occurring near 42°N on both cruises, and surface Chl *a* is highest near where the nitrate gradient is greatest (Fig. 2i,j).

The North Pacific Transition Zone (surface salinity 33.0–35.2) along 152°W was located between 30°N and 45°N during November 1997, and between 32°N and 42°N in September 2008 (Fig. 2c,d). The North Pacific Chlorophyll Front, as identified by the southern extent of the 0.2 mg m^{-3} surface chlorophyll concentration, occurred near 35–37°N on UWStu97 and near 42–44°N on UWStu08 (Fig. 3a,b). Satellite-derived chlorophyll agrees with in situ observations that the chlorophyll front was $\sim 7°$ further north in the summer. Bottle and underway sampling during the September cruise identified an $\sim$ 0.8–1.2 mg m^{-3} Chl *a* peak north of the transition zone and just north of the chlorophyll front, near 44–45°N (Fig. 2h).

The November chlorophyll front occurred during a transitional period consistent with autumn, but was further south than typical for the time of year, while the September chlorophyll front was located at its summer maximum (Fig. 3c). Due to the position of the chlorophyll front, the transition zone mixed-layer depths midway between the winter maximum of $\sim$ 150 m and the summer depth of $\sim$ 30 m, and the high winds (often $>$ 15 m s^{-1}), we characterize the November 1997 cruise as representing an autumn climatological state. We characterize the September 2008 cruise as summertime, because of the front location, shallow transition zone mixed-layer depths ($\sim$ 30 m), and generally low winds (generally $<$ 10 m s^{-1}).

Oxygen and argon supersaturation—During November 1997, mixed-layer values of surface oxygen were generally near saturation. An oxygen supersaturation maximum of $>$ 2% supersaturation at 50–90-m depth extended from 42°N in the transition zone southwards (Fig. 4a). Oxygen supersaturation generally decreased rapidly with depth below the maximum. Argon was also at or near saturation in the mixed layer, generally 0–1% supersaturated (Fig. 4c). Most stations within the subarctic frontal zone of the North Pacific Transition Zone, from 38°N to 45°N were undersaturated near the surface, likely reflecting rapid cooling in the surface water. Argon supersaturation also indicates a submixed-layer maximum at 60–100-m depth of 2–3% was present at stations from 25°N to 33°N, the

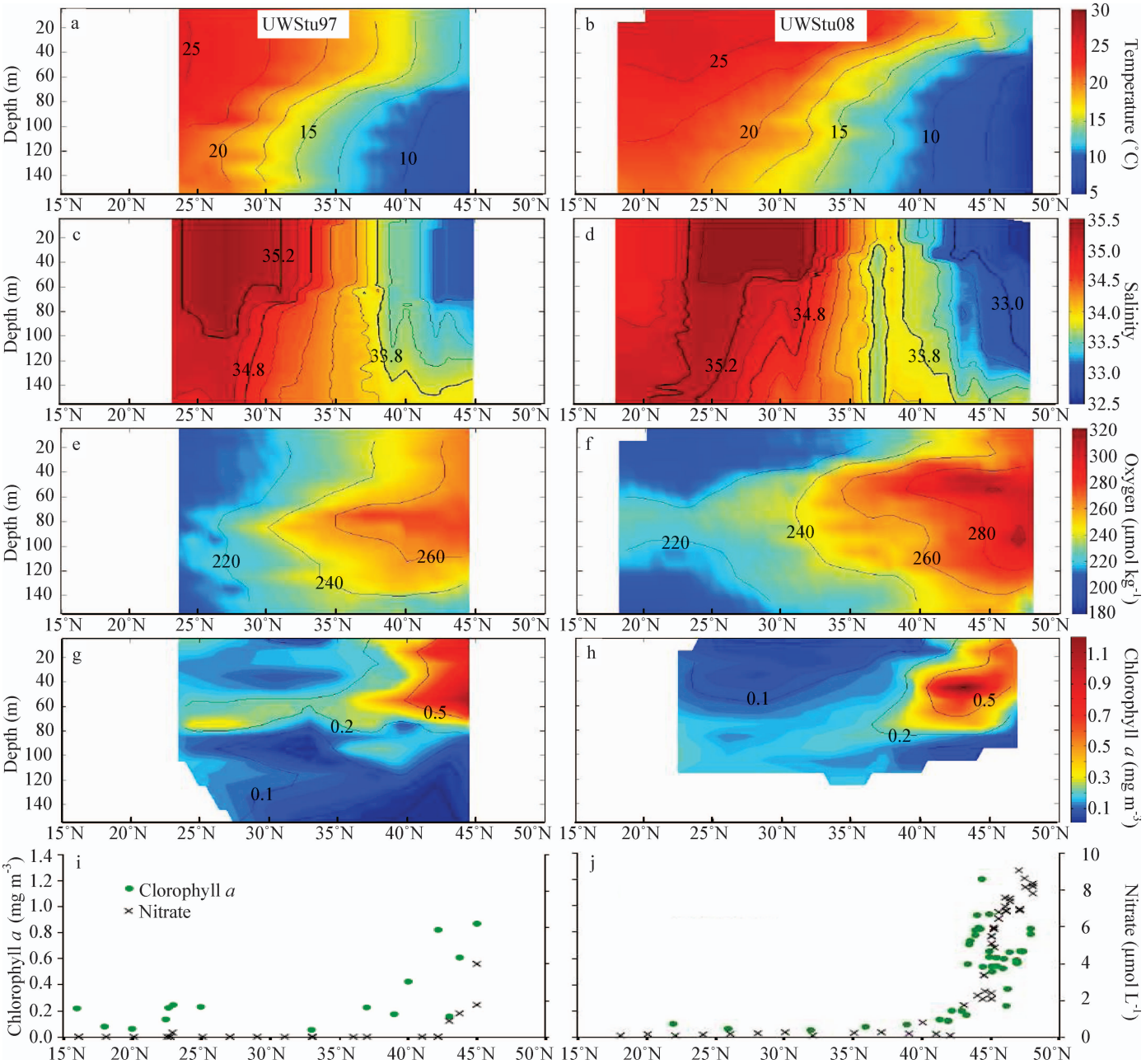

Fig. 2. Subsurface sections of physical and biological properties, and surface features of the transition region along 152°W in November 1997 (UWStu97), left column, and September 2008 (UWStu08), right column. (a,b) temperature sections. (c,d) salinity, with outcroppings of the 33.0 and 33.8 isohalines bounding the subarctic frontal zone, and isohalines of 34.8 and 35.2 bounding the subtropical frontal zone, the northern and southern limits of the North Pacific Transition Zone. (e,f) oxygen concentrations. (g,h) subsurface Chl *a*. (i,j) surface Chl *a* and nitrate.

southern portion of the transition zone into the subtropics. Below this maximum concentrations generally decreased toward saturation with depth.

Mixed-layer oxygen concentrations in September 2008 were 2–5% supersaturated, and generally more saturated further north. Stations south of 47°N in the subarctic through the subtropics were more supersaturated below the surface mixed layer, up to 4–15% between 30 m and 100 m (Fig. 4b). The maximum was of greater magnitude and extent than during the November 1997 cruise, and was most intense near the northern edge of the transition zone between 38°N and 42°N. Below this maximum, oxygen decreased with depth. Argon again followed a similar pattern with lower supersaturation. Concentrations were 1–3% above saturation in the mixed layer, with the highest values in the transition zone. Stations from 46°N through the subtropics were 2–6% supersaturated in the submixed-layer maximum (Fig. 4d). The most intense portion of the maximum again lay further south than with oxygen, between 33°N and 38°N in the transition zone, at 35–50-m

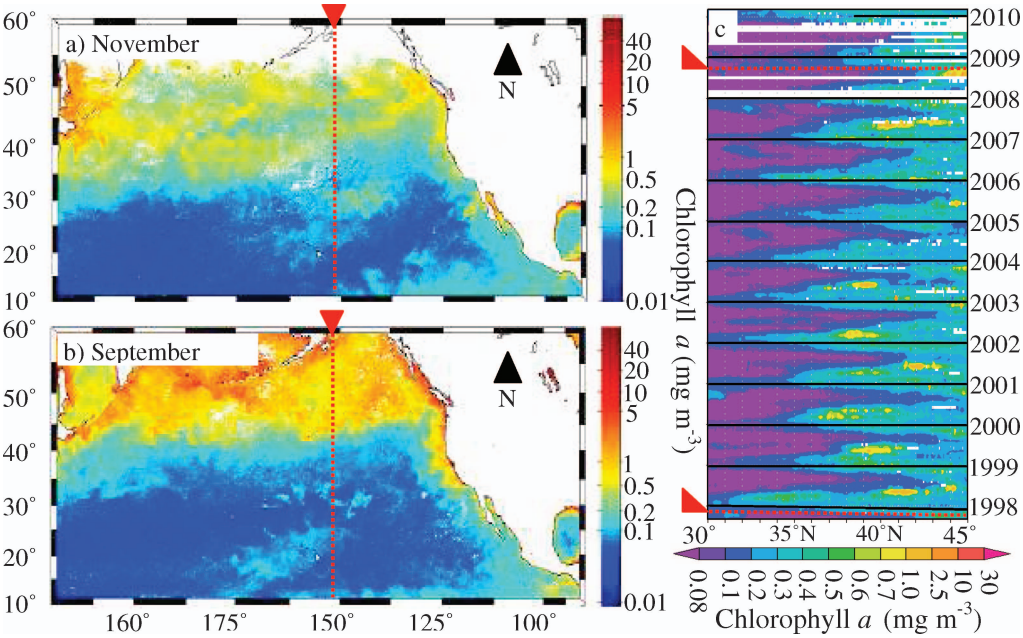

Fig. 3. NASA Sea-viewing Wide Field-of-view Sensor (SeaWiFS)–derived Chl *a* concentrations in the North Pacific during (a) November 1997 and (b) September 2008. Chlorophyll concentrations are > 0.2 mg m^{-3} from (a) $\sim$ 35–37°N and (b) north of $\sim$ 42–44°N. 152°W is identified by the red dashed lines. (c) Hovmöller diagram of surface Chl *a* made using SeaWiFS data and the NASA Giovanni remote-sensing data visualization website, with cruise months highlighted by red dashed lines.

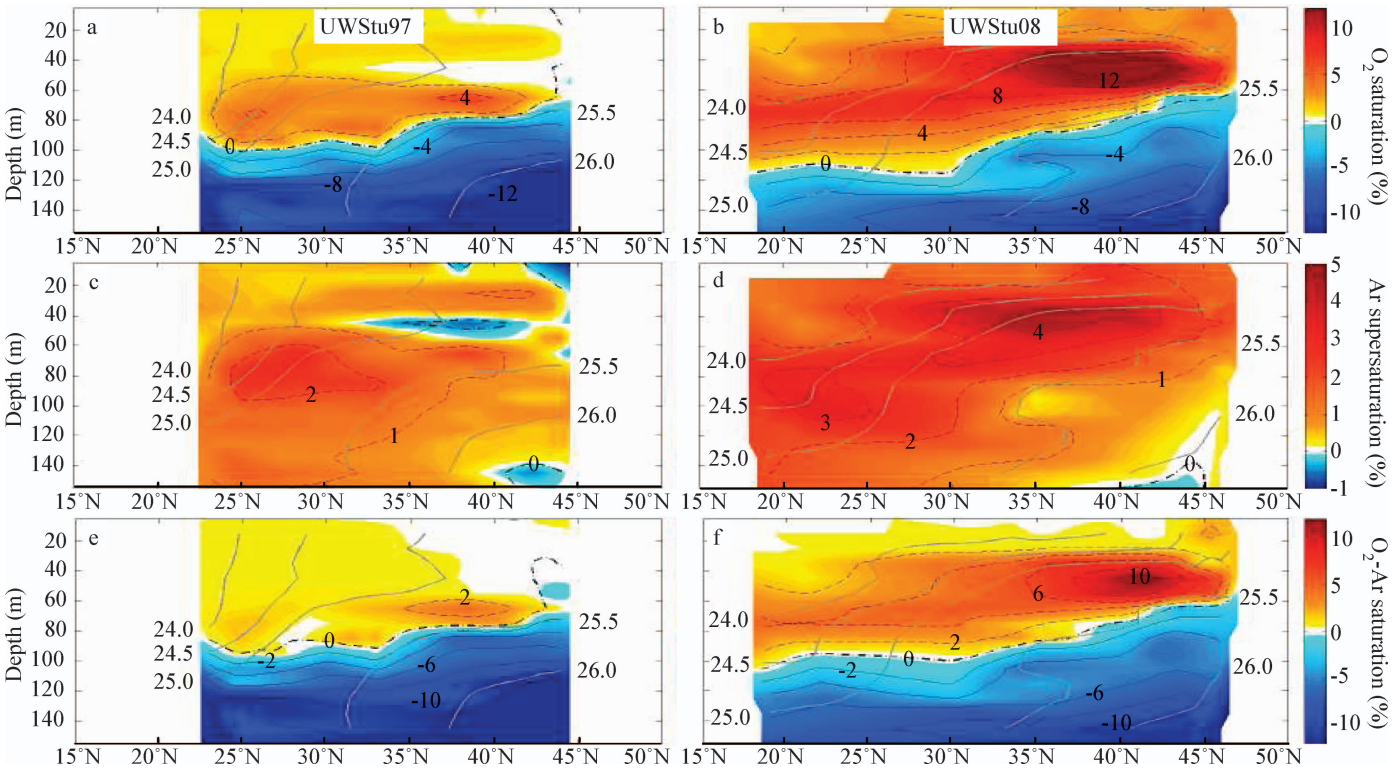

Fig. 4. Percent supersaturation for oxygen (a,b), argon (c,d) with a smaller scale, and the oxygen–argon supersaturation difference (e,f) vs. depth for November 1997 (UWStu97), left column, and September 2008 (UWStu08), right column, with density (σ_θ) plotted in gray and labeled to either side of the sections.

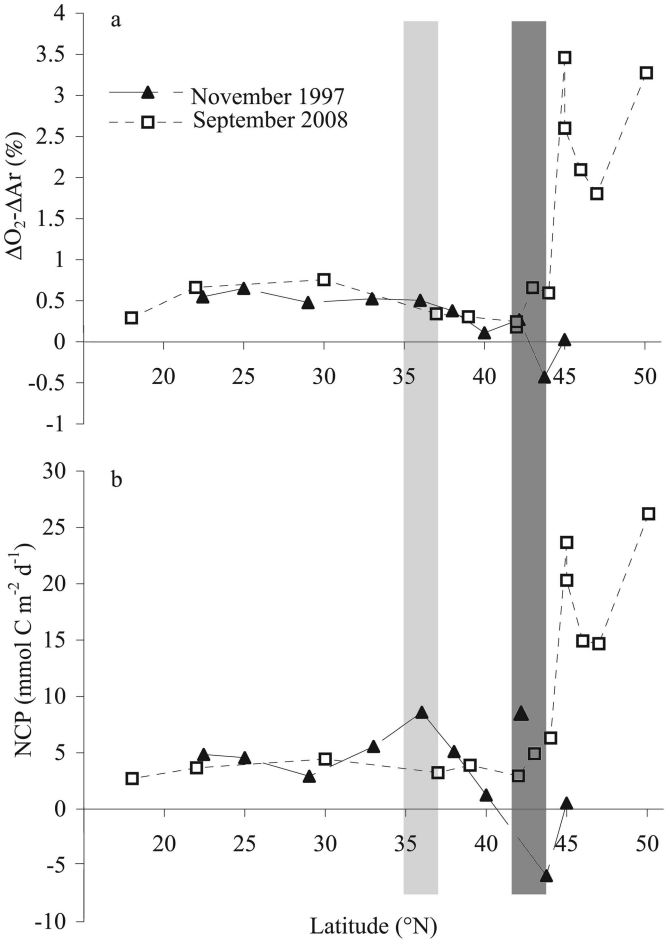

Fig. 5. (a) Surface mixed-layer $\Delta O_2 - \Delta Ar$ and (b) depth-integrated net community production of carbon for UWStu97 (triangles), and UWStu08 (squares). The lightly shaded rectangle shows the November 1997 position of the North Pacific Chlorophyll Front, while the darker rectangle shows the September 2008 NPCF, as determined by satellite imagery. November 1997 NCP at 42.2°N is not included in the plotted trend line because the difference between NCP estimates using the weighted mass transfer coefficient and a single coefficient derived from the 20-d wind-speed average is greater than the Monte Carlo–derived uncertainty in either value (*see* text).

depth. Below the supersaturation maximum, values decreased with depth toward saturation. Tables of derived oxygen and argon concentrations and hydrographic data required for their calculation are available upon request from the authors.

Positive values of the oxygen–argon supersaturation difference indicate net production (Figs. 4e,f; 5a). Surface $\Delta O_2 - \Delta Ar$ values from 40°N northward on UWStu97 were near 0%, with slight positive and negative deviations indicating little biological influence on gas supersaturation relative to physical processes over the residence time of the signal. Stations south of 40°N varied little with latitude and had values near 0.5%, or slight biological oxygen supersaturation (Fig. 5a). A submixed-layer maximum in $\Delta O_2 - \Delta Ar$ ($> 0.2\%$) on this cruise lay between 55-m and 70-m depth at 35–41°N, corresponding with submixed-layer Chl *a* and oxygen maxima and constrained between densities (σ_θ) 25.0 and 25.5 (Fig. 4e). Below this biological oxygen supersaturation decreased rapidly with depth.

Surface $\Delta O_2 - \Delta Ar$ values from September 2008 were 1.5–4% north of 44°N in the subarctic, higher than in the transition zone and the subtropics (Figs. 4f; 5a). At the northern boundary of the transition zone, surface $\Delta O_2 - \Delta Ar$ values dropped to near 0.2%, and more southern stations within the physical transition zone and subtropics varied between 0.3% and 1%, similar to observations from UWStu97. Below the mixed layer, the biological oxygen supersaturation maximum was more extensive than during November 1997, with stations between 29°N and 47°N more saturated than overlying surface waters (Fig. 4f). $\Delta O_2 - \Delta Ar$ values within the maximum were 2–14% at 25–90-m depth, again between $\sigma_\theta = 25.0$ and 25.2 and corresponding with maxima in Chl *a* and oxygen concentration. Below the maximum $\Delta O_2 - \Delta Ar$ again fell off rapidly with depth.

The $\Delta O_2 - \Delta Ar$ maxima in the transition zone are coincident with or just above (10–50 m shallower than) the nitracline, as identified by the increase in nitrate concentration above ~ 0.2 μmol NO_3^- L^{-1} (data not shown). This is consistent with the shoaling nitracline and coincident oxygen supersaturation in the region described by Hayward (1994).

Discussion

Net community production—Quantities used to calculate the surface mixed-layer production from Eq. 12 are reported in Table 1. NCP estimates from each station, in mmol O_2 m^{-2} d^{-1}, are presented in Table 2 for both the surface mixed layer and the submixed-layer depths. Depth-integrated NCP estimates are also presented in Table 2, along with mean values for each physically defined region (the subarctic Pacific, transition zone, and subtropical Pacific). We assume a production ratio of $\Delta O_2 : \Delta C = 1.45$ during photosynthesis, based on the elemental composition of pelagic plankton derived by Hedges et al. (2002), to yield an estimate of NCP in mmol C m^{-2} d^{-1}.

Uncertainties—Uncertainties in NCP are derived using independent Monte Carlo analyses for each station (Table 2). In the Monte Carlo analysis, the mass transfer coefficient, $\Delta O_2 - \Delta Ar$, advective velocity, and the quantities associated with submixed-layer production were assumed to be the primary sources of error in Eqs. 12 and 13. We assigned an uncertainty for these variables (*see* later) to be equal to $\pm$ 1 standard deviation with a Gaussian distribution about the mean. Values for these terms were chosen randomly within the distribution and the problem was solved several thousand times to obtain a mean and error for production at each station. The assumed uncertainty in the mass transfer coefficient was $\pm$ 30% based on tracer-release experiments (Reuer et al. 2007; Emerson et al. 2008). The error in $\Delta O_2 - \Delta Ar$ varied from $\pm$ 10–20% based on both duplicates and the standard deviation of all samples within the mixed layer at a given station. The uncertainty in the Ekman velocity determined from da Silva et al. (1994) wind-speeds was estimated to be

Table 2. Surface, submixed layer, and total net community production (NCP) for each station, and averages over physically demarcated regions (as in Table 2). Total depth-integrated NCP is indicated in both O_2 and C units. Individual uncertainties are calculated using a Monte Carlo analysis (*see* text). Uncertainties for the regional averages are reported as standard errors of the means. NCP of carbon was calculated from the oxygen flux assuming $\Delta O_2 : \Delta C = 1.45$ (Hedges et al. 2002).

Cruise	Latitude and longitude (°)	NCP (mmol O_2 m^{-2} d^{-1})			Total NCP (mmol C m^{-2} d^{-1})
		surface	submixed	total	
UWStu97	45N,152W	0.8±3.0	0.0±0.1	0.8±3.0	0.5±2.1
	43.7N,151.2W	−8.5±2.7	0.0±0.1	−8.5±2.7	−5.9±1.9
	42.2N,152W	12.3±6.1	0.0±0.1	12.3±6.1	8.5±4.2
	40N,152W	1.8±3.3	0.0±0.1	1.8±3.3	1.2±2.3
	38N,152W	7.1±2.4	0.3±0.4	7.4±2.4	5.1±1.7
	36N,152W	11.3±3.5	1.1±0.8	12.4±3.5	8.6±2.4
	33N,152W	7.5±2.6	0.5±0.4	8.0±2.7	5.6±1.9
	29N,152W	4.1±2.3	0.1±0.1	4.2±2.3	2.9±1.6
	25N,152W	6.4±2.1	0.2±0.3	6.6±2.1	4.6±1.5
	22.4N,158.1W	7.0±2.3	0.0±0.1	7.0±2.3	4.9±1.6
North Pacific Transition Zone	(30–45°N)	4.6±2.7	0.3±0.2	4.9±2.8	3.4±2.0
Subtropical Pacific	(<30°N)	5.8±0.9	0.1±0.1	5.9±0.9	4.1±0.6
UWStu08	50.1N,144.8W	37.4±10.9	0.5±0.6	37.8±10.9	26.2±7.6
	47N,152W	21.2±6.4	0.0±0.1	21.2±6.6	14.7±4.6
	46N,150.6W	21.4±6.6	0.1±0.1	21.6±6.7	14.9±4.6
	45N,152W	29.2±9.1	0.2±0.2	29.3±9.2	20.3±6.4
	45N,149.9W	34.1±10.0	0.0±0.1	34.2±10.0	23.7±6.9
	44N,149.2W	4.0±1.9	5.1±2.2	9.1±2.4	6.3±1.7
	43N,148.5W	4.8±1.9	2.3±0.6	7.1±1.9	4.9±1.3
	42N,152W	1.4±0.5	2.9±1.6	4.3±1.6	2.9±1.1
	42N,145W	2.3±0.8	2.0±1.4	4.3±1.6	2.9±1.1
	39N,152W	2.2±1.2	3.4±1.4	5.6±1.8	3.9±1.2
	37N,152W	2.3±2.1	2.4±0.8	4.7±2.3	3.2±1.6
	30N,152W	5.0±1.6	1.5±0.6	6.4±1.8	4.4±1.2
	22N,152W	5.2±1.6	0.1±0.1	5.3±1.6	3.7±1.1
	18N,152W	2.7±1.0	1.3±0.6	3.9±1.3	2.7±0.9
Subarctic Pacific	(>42°N)	21.7±5.0	1.2±0.7	22.9±4.5	15.9±3.1
North Pacific Transition Zone	(32–42°N)	2.0±0.2	2.7±0.3	4.7±0.3	3.3±0.2
Subtropical Pacific	(<32°N)	4.3±0.8	0.9±0.4	5.2±0.7	3.6±0.5

± 20% (MacCready and Quay 2001). The error in the submixed-layer $\Delta O_2 - \Delta Ar$ reservoir was rather large, ± 50%, because of assumptions about the depth integral and the duration of the increase.

The uncertainty in the flux estimates derived from the Monte Carlo analysis averaged ± 37% for UWStu97, but was much higher at stations with high winds or low production. UWStu08 subarctic and subtropical flux uncertainties averaged ± 32%, while transition-zone estimates were less certain. The sources of error contributed differently to the total Monte Carlo analysis. The uncertainty in the mass transfer coefficient accounted on average for 50% (UWStu97) and 60% (UWStu08) of the flux error, surface $\Delta O_2 - \Delta Ar$ for 45% (UWStu97) and 10% (UWStu08), and the Ekman velocity for < 2% on both cruises. Submixed-layer errors averaged 5% (UWStu97) and 25% (UWStu08) of the total, but were much higher in the September 2008 transition zone. These stations generally had lower mixed-layer production and higher submixed-layer production than elsewhere. The uncertainty for each regional average in Table 2 is calculated as the standard error of the mean.

Because the error in the gas exchange rate is large, we estimated the effect of using the weighted moving-average method of Reuer et al. (2007) for determining the mass transfer coefficient from wind speed. If a simple averaging of wind speeds over the 20 d prior to sampling was used instead of the weighted average, NCP was 27% and 13% lower during UWStu97 and UWStu08, respectively. The only station where the difference between the two methods of calculation was greater than the uncertainty of the result was at 42.2°N in November 1997. At this location, the 20-d average k_{O2} was almost 8 m d^{-1} smaller than the 60-d weighted mass transfer coefficient. The satellite-determined wind-speed at this location was ~ 35 m s^{-1} at 42.2°N on 06 November 1997, 2 d prior to sampling. This was much higher than the 9 m s^{-1} average in the preceding 20 d. The rapid change to non–steady-state conditions probably biased the estimated flux during this storm, and for this reason we omitted the station at 42.2°N from the NCP trend line in Fig. 5b.

Regional trends and comparison with literature values—NCP differences between the cruises described here,

separated by slightly more than 10 yr, are assumed to represent seasonal rather than interannual trends because seasonal variability in the pelagic North Pacific is far greater than that caused by longer term cycles like El Niño and the Pacific Decadal Oscillation (Emerson 1987; Keeling et al. 2004). Average NCP values in the subtropical ocean were low and similar between November 1997 and September 2008 (4.1 ± 0.6 and 3.6 ± 0.5 mmol C m^{-2} d^{-1}, respectively; Table 2). These averages are similar to the seasonal production estimate from the VOS cruises described by Juranek (2007), who determined a mean value for March, April, and October of 4.9 mmol C m^{-2} d^{-1}, and they are at the low end of annual estimates at Sta. ALOHA ($\bar{x}$ 6.7 ± 2.6 mmol C m^{-2} d^{-1}; Emerson et al. 2008). Transition-zone NCP determined on our cruises was similar to the subtropical values, and indistinguishable between November 1997 and September 2008 given the errors in the estimates (3.4 ± 2.0, UWStu97 and 3.3 ± 0.2 mmol C m^{-2} d^{-1}, UWStu08); however, they are much lower than the value of 14.2 mmol C m^{-2} d^{-1} determined by Juranek (2007) in the region. NCP was not determined in the subarctic Pacific on the November 1997 cruise, but the value measured in September 2008, 15.9 ± 3.1 mmol C m^{-2} d^{-1}, was around four times greater than production observed in the subtropics and transition zone during either season. High production values in the area of Sta. P (50°N) in September 2008 may reflect unusually high phytoplankton bloom conditions reported across the entire subarctic Pacific (Hamme et al. 2010).

Submixed-layer production varied greatly with season and region. In November 1997 it was negligible north of the subarctic frontal zone (38°N), and accounted on average for 5% of the total through the rest of the transition zone and the subtropics. September 2008 submixed-layer production was again negligible in the subarctic, but accounted for 18% of total NCP in the subtropics and 57% of the total in the transition zone, where the depth-integrated production was relatively low. Such high submixed-layer production in this region indicates that satellite-derived primary productivity values are probably underestimates in the subtropical gyre, where satellite-based ocean color sensors may not detect submixed-layer chlorophyll maxima at tens of meters depth.

The North Pacific Chlorophyll Front and regional production—Although the highest NCP values observed in September 2008 were in the subarctic and not the transition zone as defined by salinity criteria, production during this cruise peaked just north of the transition zone, near the North Pacific Chlorophyll Front. There are maxima in biological production at or just north of the chlorophyll front in both seasons (Fig. 5b). Average production at the November 1997 chlorophyll front (35–37°N) was 6.4 ± 1.1 mmol C m^{-2} d^{-1} ($\bar{x}$ of 33°N, 36°N, and 38°N), 1.5–2 times higher than in adjacent waters. In September 2008, peak production was between 44°N and 46°N, just north of the chlorophyll front (near 42–44°N), and was 16.3 ± 3.8 mmol C m^{-2} d^{-1} ($\bar{x}$ of 44–46°N). Production maxima at or near the North Pacific Chlorophyll Front were a persistent feature of these cruises, and the observed latitudinal variation suggests the seasonal shift in NCP is associated with the chlorophyll front rather than the physical subarctic–subtropical boundary, which is relatively immobile (Roden 1991).

Table 3. Estimates of net air–water CO_2 fluxes and net community production (NCP) of carbon in the 30–45°N region for autumn (Oct, Nov, and Dec), summer (Jul, Aug, Sep) or seasonally from spring through early autumn, and annually. Seasons are defined after Zeng et al. (2002). The method used in each study is noted in the footnotes. Uncertainties are reported as standard errors of the means.

Season	Flux (mmol C m^{-2} d^{-1})	
	Air–water CO_2 flux	NCP
Autumn	5.9*	3.4±2.0†
Summer (or seasonal)	1.3*	8.1±2.7†, 14.2‡, 14.6§
Annual	3.9*, 5.5–8.2‖	—

* pCO_2 drawdown, 34–53°N across Pacific (Zeng et al. 2002).
† O_2:Ar and biological O_2 mass balance (this study).
‡ O_2:Ar and biological O_2 mass balance, Mar, Apr, Oct mean (Juranek 2007).
§ NO_3^- drawdown in 'Transition Domain,' ~ 40–45°N across Pacific, Mar–Sep (Wong et al. 2002).
‖ pCO_2 drawdown, ~ 30–45°N (Takahashi et al. 2009).

The importance of NCP in the total CO_2 drawdown of the gyre boundary region is a central concern of this study. To compare our results with those from climatological pCO_2 data and other regional NCP estimates, we averaged over the full annual range of the chlorophyll front, ~ 30–45°N (Fig. 3). This region is identical to the transition zone in November 1997, but is 5° wider than the transition zone in 2008. The pCO_2 minimum in the 30–45°N region is strongest in the autumn, when both biological carbon export and sea-surface cooling create a strong pCO_2 difference between the atmosphere and surface ocean (Zeng et al. 2002; Takahashi et al. 2009). CO_2 drawdown is weakest in summer, when warming tends to cause pCO_2 saturation and counteracts the biological pump (Zeng et al. 2002).

Takahashi et al. (2002, 2009) suggest that temperature effects dominate the net CO_2 fluxes in the 30–45°N region during both seasons; however, our results indicate that biological production is an important component of the CO_2 drawdown in both seasons (Table 3). Our estimate of November 1997 NCP (3.4 ± 2.0 mmol C m^{-2} d^{-1}) is greater than half the magnitude of the net air–water CO_2 flux in the region, although the uncertainties are large. September 2008 NCP is greater, 8.1 ± 2.7 mmol C m^{-2} d^{-1}, and must exceed summertime temperature-induced outgassing to explain the net CO_2 influx measured by Zeng et al. (2002). Previous seasonal NCP estimates for the 30–45°N region by Wong et al. (2002) and Juranek (2007) are even greater than ours. Because much of the NCP from 30°N to 45°N is at the chlorophyll front (Fig. 5b), the biological pump in the vicinity of the front plays a large role in this region. Some factor(s) not directly associated with the physically defined transition zone must determine production in the chlorophyll front. Ayers and Lozier (2010) estimate that nitrate convergence in the transition zone (30–40°N) supports an autumn (Oct, Nov, and Dec) NCP of

0.6 mmol C m^{-2} d^{-1} over the entire region, but there is a wintertime peak of ~ 4 mmol C m^{-2} d^{-1} in the zone of maximum convergence (J. Ayers pers. comm.). The peak value is of the same magnitude as the 3.4 ± 2.0 mmol C m^{-2} d^{-1} measured on UWStu97, but the area-wide estimate is only ~ 20% of the value we estimate for the 30–45°N region (Table 3). As mentioned above, our regional values are on the low end of annual production estimates from ocean time-series data in the subtropics and subarctic, so the actual proportion of autumn production supported by nitrate convergence may be lower. Another possible nitrate source is from vertical mixing with water below the mixed layer. The nitracline in the subtropics is too deep for mixing to access nutrient-rich waters, but it was found at 70–120 m from 30°N to 45°N during our cruise (data not shown), which is consistent with climatology in this area (Hayward 1994). Because nitrate concentrations in the surface waters are low, it is also possible that nitrogen is supplied by nitrogen fixation, a potentially iron-limited process (Mills et al. 2005; Ayers and Lozier 2010).

The primary motivation for this study was to clarify the role of biological production in creating the observed CO_2 drawdown in the subarctic–subtropical boundary region. Our NCP estimates indicate that the biological pump plays an important role in the 30–45°N region of the eastern North Pacific, both when the pCO_2 is near maximum undersaturation and when it is near saturation. The chlorophyll front may contribute significantly to regional production, although the nutrient sources fueling it remain ambiguous. Because of the magnitude of the biological and physical fluxes involved, changes to the balance of the system caused by climate forcing could significantly affect the seasonal and annual sinks for carbon in this region.

Acknowledgments

Thanks to K. Tempest for assistance in obtaining and processing satellite wind-speed data, the crew of the R/V *Thompson* for cruise operations, and to those who carefully reviewed and edited this manuscript. This research was supported through National Science Foundation Ocean Sciences grant 0628663 and the University of Washington School of Oceanography.

References

Abell, J. 2003. Quantifying the role of dissolved organic matter in the cycling of carbon, oxygen and nutrients in the upper ocean. Ph.D. thesis. Univ. of Washington.

Aydin, M., Z. Top, and D. Olson. 2004. Exchange processes and watermass modifications along the subarctic front in the North Pacific: Oxygen consumption rates and net carbon flux. J. Mar. Res. **62:** 153–167, doi:10.1357/002224004774201672

Ayers, J., and M. Lozier. 2010. Physical controls on the seasonal migration of the North Pacific Transition Zone Chlorophyll Front. J. Geophys. Res. **115:** C05001, doi:10.1029/2009JC005596

Brinton, E. 1962. The distribution of euphausiids. Bull. Scripps Inst. Oceanogr. **8:** 51–270.

Carpenter, J. 1965. The Chesapeake Bay Institute technique for the Winkler dissolved oxygen method. Limnol. Oceanogr. **10:** 141–143, doi:10.4319/lo.1965.10.1.0141

Craig, H., and T. Hayward. 1987. Oxygen supersaturation in the ocean: Biological vs. physical contributions. Science **235:** 199–202, doi:10.1126/science.235.4785.199

da Silva, A., C. Young, and S. Levitus. 1994. Atlas of surface marine data 1994, v. 1: Algorithms and procedures. NOAA Atlas NESDIS 6.

Emerson, S. 1987. Seasonal oxygen cycles and biological new production in surface waters of the subarctic Pacific Ocean. J. Geophys. Res. **92:** 6535–6544, doi:10.1029/JC092iC06p06535

———, and J. Hedges. 2008. Chemical oceanography and the marine carbon cycle. Cambridge Univ. Press.

———, P. Quay, C. Stump, D. Wilbur, and M. Knox. 1991. O_2, Ar, N_2, and ^{222}Rn in surface waters of the subarctic ocean: Net biological O_2 production. Glob. Biogeochem. Cycles **5:** 49–69, doi:10.1029/90GB02656

———, ———, ———, ———, and R. Schudlich. 1995. Chemical tracers of productivity and respiration in the subtropical Pacific Ocean. J. Geophys. Res. **100:** 15873–15887, doi:10.1029/95JC01333

———, and C. Stump. 2010. Net biological oxygen production in the ocean II: Remote in situ measurements of O_2 and N_2 in subarctic Pacific surface waters. Deep-Sea Res. I **57:** 1255–1265, doi:10.1016/j.dsr.2010.06.001

———, ———, and D. Nicholson. 2008. Net biological oxygen production in the ocean: Remote in situ measurements of O_2 and N_2 in surface waters. Glob. Biogeochem. Cycles **22:** GB3023, doi:10.1029/2007GB003095

———, ———, D. Wilbur, and P. Quay. 1999. Accurate measurement of O_2, N_2, and Ar gases in water and the solubility of N_2. Mar. Chem. **64:** 337–347, doi:10.1016/S0304-4203(98)00090-5

Fuchs, G., W. Roether, and P. Schlosser. 1987. Excess ^3He in the ocean surface layer. J. Geophys. Res. **92:** 6559–6568, doi:10.1029/JC092iC06p06559

Hamme, R., and S. Emerson. 2006. Constraining bubble dynamics and mixing with dissolved gases: Implications for productivity measurements by oxygen mass balance. J. Mar. Res. **64:** 73–95, doi:10.1357/002224006776412322

———, and others. In press. Volcanic ash fuels anomalous plankton bloom in subarctic northeast Pacific. Geophys. Res. Lett. **37:** L19604, doi:10.1029/2010GL044629

Hayward, T. 1994. The shallow oxygen maximum layer and primary production. Deep-Sea Res. I **41:** 559–574, doi:10.1016/0967-0637(94)90095-7

Hedges, J., J. Baldock, Y. Gelinas, C. Lee, M. Peterson, and S. Wakeham. 2002. The biochemical and elemental compositions of marine plankton: An NMR perspective. Mar. Chem. **78:** 47–63, doi:10.1016/S0304-4203(02)00009-9

Juranek, L. 2007. Assessment of Pacific Ocean organic carbon production and export using measurements of dissolved oxygen isotopes and oxygen/argon gas ratios. Ph.D. thesis. Univ. of Washington.

Keeling, C., H. Brix, and N. Gruber. 2004. Seasonal and long-term dynamics of the upper ocean carbon cycle at Station ALOHA near Hawaii. Glob. Biogeochem. Cycles **18:** GB4006, doi:10.1029/2004GB002227

Knap, A., A. Michaels, A. Close, H. Ducklow, and A. Dickson [eds.]. 1996. Protocols for the Joint Global Ocean Flux Study (JGOFS) core measurements. Reprint, UNESCO 1994 IOC Manuals and Guides **29**.

Laurs, R., and R. Lynn. 1991. North Pacific albacore ecology and oceanography. NOAA Tech. Rep. **105:** 69–88.

Lynn, R. 1986. The subarctic and northern subtropical fronts in the eastern North Pacific Ocean in the spring. J. Phys. Oceanogr. **16:** 209–222, doi:10.1175/1520-0485(1986)016<0209:TSANSF>2.0.CO;2

Maccready, P., and P. Quay. 2001. Biological export flux in the Southern Ocean estimated from a climatological nitrate budget. Deep-Sea Res. II **48:** 4299–4322, doi:10.1016/S0967-0645(01)00090-X

Mills, M., C. Ridame, M. Davey, J. La Roche, and R. Geider. 2005. Iron and phosphorous co-limit nitrogen fixation in the eastern tropical North Atlantic. Nature **437:** 292–294.

Nicholson, D., S. Emerson, and C. Eriksen. 2008. Net community production in the deep euphotic zone of the subtropical North Pacific gyre from glider surveys. Limnol. Oceanogr. **53:** 2226–2236.

Nightingale, P., and others. 2000. In situ evaluation of air–sea gas exchange parameterizations using novel conservative and volatile tracers. Glob. Biogeochem. Cycles **14:** 373–387, doi:10.1029/1999GB900091

Pearcy, W. 1991. Biology of the transition region. NOAA Tech. Rep. **105:** 39–55.

Polovina, J., E. Howell, D. Kobayashi, and M. Seki. 2001. The transition zone chlorophyll front, a dynamic global feature defining migration and forage habitat for marine resources. Prog. Oceanogr. **49:** 469–483, doi:10.1016/S0079-6611(01)00036-2

Reuer, M., B. Barnett, M. Bender, P. Falkowski, and M. Hendricks. 2007. New estimates of southern ocean biological production rates from O_2/Ar ratios and triple isotope composition of O_2. Deep-Sea Res. I **54:** 951–974, doi:10.1016/j.dsr.2007.02.007

Roden, G. 1991. Subarctic–subtropical transition zone of the North Pacific: Large-scale aspects and mesoscale structure. NOAA Tech. Rep. **105:** 1–38.

Spitzer, W., and W. Jenkins. 1989. Rates of vertical mixing, gas exchange and new production: Estimates from seasonal gas cycles in the upper ocean near Bermuda. J. Mar. Res. **47:** 169–196, doi:10.1357/002224089785076370

Takahashi, T., and others. 2002. Global sea–air CO2 flux based on climatological surface ocean *p*CO2, and seasonal biological and temperature effects. Deep-Sea Res. II **49:** 1610–1622.

———, and ———. 2009. Climatological mean and decadal change in surface ocean pCO_2, and net sea–air CO_2 flux over the global oceans. Deep-Sea Res. II **56:** 554–557, doi:10.1016/j.dsr2.2008.12.009

Volk, T., and M. Hoffert. 1985. Ocean carbon pumps: Analysis of relative strengths and efficiencies in ocean-driven atmospheric changes, 99–110. *In* E. Sundquist and W. Broecker [eds.], The carbon cycle and atmospheric CO_2: Natural variations Archean to present. Geophys. Monogr. Am. Geophys. Union **32**.

Wanninkhof, R. 1992. Relationship between wind speed and gas exchange over the ocean. J. Geophys. Res. **97:** 7373–7382, doi:10.1029/92JC00188

Wijffels, S., E. Firing, and H. Bryden. 1994. Direct observations of the Ekman balance at 10°N in the Pacific. J. Phys. Oceanogr. **24:** 1666–1679, doi:10.1175/1520-0485(1994)024<1666:DOOTEB>2.0.CO;2

Wong, C., D. Waser, F. Nojiri, A. Whitney, J. Page, and J. Zeng. 2002. Seasonal cycles of nutrients and dissolved inorganic carbon at high and mid latitudes in the North Pacific Ocean during the Skaugran cruises: Determination of new production and nutrient uptake ratios. Deep-Sea Res. II **49:** 5317–5338, doi:10.1016/S0967-0645(02)00193-5

Zeng, J., Y. Nojiri, P. Murphy, C. Wong, and Y. Fujinuma. 2002. A comparison of ΔpCO_2 distributions in the northern North Pacific using results from a commercial vessel in 1995–1999. Deep-Sea Res. II **49:** 5303–5315, doi:10.1016/S0967-0645(02)00192-3

Associate editor: Michael R. Landry

Received: 20 January 2010
Accepted: 02 August 2010
Amended: 20 August 2010